nature communications

Article

https://doi.org/10.1038/s41467-024-54529-y

SPLICER: a highly efficient base editing toolbox that enables in vivo therapeutic exon skipping

Received: 15 December 2023

Accepted: 13 November 2024

Published online: 28 November 2024

Check for updates

Angelo Miskalis[1,6], Shraddha Shirguppe[1,6], Jackson Winter[1,6], Gianna Elias[1], Devyani Swami[1], Ananthan Nambiar[1,2], Michelle Stilger[1], Wendy S. Woods[1], Nicholas Gosstola[1,2], Michael Gapinske[1], Alejandra Zeballos[1], Hayden Moore[1], Sergei Maslov[1,2], Thomas Gaj[1,2] & Pablo Perez-Pinera[1,2,3,4,5]

Exon skipping technologies enable exclusion of targeted exons from mature mRNA transcripts, which have broad applications in medicine and biotechnology. Existing techniques including antisense oligonucleotides, targetable nucleases, and base editors, while effective for specific applications, remain hindered by transient effects, genotoxicity, and inconsistent exon skipping. To overcome these limitations, here we develop SPLICER, a toolbox of next-generation base editors containing near-PAMless Cas9 nickase variants fused to adenosine or cytosine deaminases for the simultaneous editing of splice acceptor (SA) and splice donor (SD) sequences. Synchronized SA and SD editing improves exon skipping, reduces aberrant splicing, and enables skipping of exons refractory to single splice site editing. To demonstrate the therapeutic potential of SPLICER, we target *APP* exon 17, which encodes amino acids that are cleaved to form Aβ plaques in Alzheimer's disease. SPLICER reduces the formation of Aβ42 peptides in vitro and enables efficient exon skipping in a mouse model of Alzheimer's disease. Overall, SPLICER is a widely applicable and efficient exon skipping toolbox.

Programmable genome-editing nucleases have fundamentally transformed biotechnology and medicine by providing a facile means to introduce targeted modifications in the genome of living cells[1]. Nonetheless, their reliance on DNA double-strand breaks (DSBs) has been linked to undesirable effects, including chromosomal deletions[2], chromothripsis[3], activation of the p53-mediated DNA damage response pathway[4], and mRNA misregulation[5], all of which can hinder their implementation[6,7]. For these reasons, emergent gene editing technologies capable of introducing precise and predictable mutations without DSBs are becoming increasingly adopted for a range of applications.

One such technology are base editors (BEs), which utilize a fusion of a Cas9 nickase and a cytosine deaminase to introduce C-to-T (cytosine base editors; CBEs) or an adenosine deaminase (adenosine base editors; ABEs) to introduce A-to-G mutations at genomic loci with complementarity to a single-guide RNA (sgRNA)[8,9]. One application of BEs is the programmable modulation of RNA splicing, which can be used to modify the transcriptional landscape of a cell for basic biology and therapeutic applications. For this goal, we previously described CRISPR-SKIP, a technology that relies on BEs to target and mutate highly conserved AG dinucleotide motifs in splice acceptor (SA) sequences, which can prevent their recognition by the spliceosome

[1]The Grainger College of Engineering, Department of Bioengineering, University of Illinois Urbana-Champaign, Urbana, IL, USA. [2]Carl R. Woese Institute for Genomic Biology, University of Illinois Urbana-Champaign, Urbana, IL, USA. [3]Department of Biomedical and Translational Sciences, Carle-Illinois College of Medicine, University of Illinois Urbana-Champaign, Urbana, IL, USA. [4]Cancer Center at Illinois, University of Illinois Urbana-Champaign, Urbana, IL, USA. [5]Department of Molecular and Integrative Physiology, University of Illinois Urbana-Champaign, Urbana, IL, USA. [6]These authors contributed equally: Angelo Miskalis, Shraddha Shirguppe, Jackson Winter. e-mail: pablo@illinois.edu

and induce skipping of the corresponding exon[10]. In addition to our work, others have utilized SpCas9 to introduce exon skipping by mutating splice donor (SD) sites and have applied BEs to induce exon skipping for various applications[11–15]. Notably, by excluding exons from mature mRNA transcripts, CRISPR-SKIP and other approaches for exon skipping hold the potential to eliminate mutated sequences and recover reading frames lost to chromosomal deletions.

Nonetheless, multiple challenges exist that prevent the broad implementation of SpCas9-comprised BEs for exon skipping. First, the native SpCas9 protein can only target splice sites with NGG protospacer adjacent (PAM) motifs nearby the target locus[1,16], a restriction that can limit the number of exons that can be effectively engaged. Second, the adenosine and cytosine deaminase domains most commonly used in first-generation BEs possess context-dependent preferences that can prevent the effective editing of a range of splice sites[1,17,18]. Third, even when SpCas9 BE technologies are able to edit splice sites, there exist in many exons cryptic splice sites that can be recognized by the spliceosome, which can lead to partial skipping[13,19,20]. Further, in addition to cryptic splicing sequences, the targeting of SA or SD sites can lead to the partial or full retention of introns in mature transcripts, which can result in the incorporation of novel sequences into open reading frames or create early termination codons that could undesirably repress expression[19–23].

To overcome these limitations, here we report SPLICER (**S**ynchronized **P**AM-less sp**L**ice s**I**te **C**onversion with bas**E** edito**R**s), a toolbox of near-PAMless CRISPR-Cas9 BEs comprised of enhanced deaminase domains that enable the simultaneous targeting of SD and SA sites, which we show improves exon skipping, reduces aberrant splicing outcomes, including cryptic splicing and intron retention, and enables the skipping of exons previously found to be resilient to skipping. Further, to highlight the potential of this toolbox, we demonstrate that SPLICER can be used to induce skipping of exon 17 in the gene encoding the amyloid precursor protein (APP), a transmembrane receptor that contributes to the formation of the amyloid deposits in the brain of patients afflicted by Alzheimer's disease[24–30]. SPLICER reduces the formation of Aβ42 peptides in vitro and mediates efficient exon skipping in a mouse model of Alzheimer's disease.

Given its precision, versatility and efficacy, we believe SPLICER will have broad applications in medicine and biotechnology.

Results

Engineered near-PAMless SpCas9 variants enable targeting of SAs inaccessible by the wild-type SpCas9

One limitation of SpCas9 for exon skipping is its reliance on the NGG PAM motif. We previously demonstrated that the use of SaCas9 or SpCas9-VQR could alleviate this problem, but BEs comprised of these variants often exhibit lower activity than those composed of the wild-type (WT) SpCas9[10,31]. Recently, several versions of SpCas9 with relaxed PAM preferences have been developed, including SpCas9-NG (NG PAM)[32], xCas9-NG (NG PAM)[33,34], NAG-Cas9 (NRG PAM)[35], SpCas9-NRNH (NRNH PAM)[36], SpG Cas9 (NRN PAM)[37], and SpRY Cas9 (near NNN PAM)[37]. Most notably, SpRY Cas9 has demonstrated DNA editing activity at NRN and NYN PAM sites comparable to SpCas9 targeted to its native PAM[37]. SpRY Cas9 was also demonstrated to edit a larger number of targets than xCas9-NG, SpCas9-NG, and SpG Cas9[37]. Therefore, we hypothesized that SpRY Cas9, by enabling tiling of splicing sequences with multiple sgRNAs, could enhance exon skipping with BEs (Fig. 1A).

To determine whether SpRY Cas9 can expand a BE toolbox to genes with noncanonical PAMs as well as edit genes with canonical PAMs at similar or higher rates than SpCas9, we designed sgRNAs tiling SAs of exons in six genes with both NGG and noncanonical PAMs (*TRAP1* exon 4, *RAB34* exon 9, *COL4A5* exon 21, *APP* exon 17, *JAG1* exon 12, and *EGFR* exon 23). These sgRNAs were delivered with SpCas9 or SpRY Cas9 BEs fused with either the adenosine deaminase ABE8e[38] (Fig. 1B, C) or the cytosine deaminase CBE4max (Fig. 1D, E). Three of these exons contained NGG / NAG PAM motifs for both ABEs and CBEs *(TRAP1* exon 4, *EGFR* exon 23, and *JAG1* exon 12*)*. The other three exons *(RAB34* exon 9, *COL4A5* exon 21, and *APP* exon 17) either lacked canonical NGG PAMs *(APP* exon 17*)* or contained one potential NGG PAM enabling targeting by CBEs but not ABEs or vice-versa.

Overall, for all sites with editing of at least 5%, the mean editing efficiencies for SpRY-ABE8e and SpRY-CBE4max were ~31% and ~35%, respectively, while the efficiencies for SpCas9 ABE8e and SpCas9 CBE4max were ~3% for each, which corresponds to a ~ 9.5- and ~9.7-fold increase in efficiency for SpRY compared to SpCas9 for both ABE8e and CBE4max, respectively (Fig. 1C, E). For the ABE8e and CBE4max variants fused with SpRY Cas9, we identified at least one sgRNA per exon that introduced the desired mutation at every target while the equivalent SpCas9 BEs edited three of the six exons, and only with sgRNAs containing NGG or NAG PAMs (Fig. 1B–E). For SpRY-ABE8e and SpRY-CBE4max, 81% and 60% of the active sgRNAs contained a non-canonical PAM respectively. SpCas9-ABE8e was able to edit two targets with NAG PAMs while SpCas9-CBE4max edited one target with an NGG PAM. For these sgRNAs, SpRY Cas9 showed higher editing efficiencies than SpCas9 at the CBE site (Fig. 1B, D) and edited at similar rate for the ABE site (Fig. 1B, D). Thus, SpRY Cas9-BEs enable editing of SAs of exons that were previously refractory to targeting with SpCas9 ($p < 0.001$; Fig. 1C, E).

An important parameter for optimizing editing of a splicing sequence with a BE is the selection of the deaminase domains, as multiple new Cas9 BEs have been developed for various purposes. For example, in addition to CBE4max[39], CBEs composed of the evoFERNY[40], SsAPOBEC3B (R54Q)[41], RrA3F (F130L)[41], TadCBEd[42], and PpAPOBEC1 (H122A)[41] catalytic domains have expanded editing contexts, increased overall editing efficiency, and decreased non-specific deamination. In the case of ABEs, evolved variants such as the ABE8[43] family, including ABE8e[44] and ABE8.20m[43], have increased editing efficiency and offer unique editing windows compared to ABE7.10[43]. Additionally, ABE9[45] was developed to further minimize bystander editing. Given the increased number of deaminase domains with unique properties, we sought to determine if we could increase DNA editing activity at the SA as well as increase the number of functioning sgRNAs.

When fusing the deaminases mentioned above to SpRY Cas9, we observed different profiles of edited SA sequences for each deaminase (Fig. 1F–I). To ensure that the differences in base editing were due to the different properties of the deaminases and not to large differences in BE protein expression levels, we performed western blots with anti-Cas9 antibodies for ABEs (Fig. S1A, B) and CBEs (Fig. S1C, D). To account for any differences in editing due to levels of protein expression, we normalized all editing levels to the normalized expression of each BE. When comparing ABEs, ABE8e outperformed all other deaminases and had a mean editing rate of ~47% compared to ~7%, ~28%, and ~0.3% for ABE7.1, ABE8.20m, and ABE9, respectively ($p < 0.05$, Fig. 1F, G), which correlates well with previous studies demonstrating the superior editing activities of ABE8e[44] and ABE8.20m[43].

Comparison of different CBEs demonstrated significant differences in mean editing rates between CBE4max and SsAPOBEC3B (R54Q) and CBE4max and PpAPOBEC1 (H122A) ($p < 0.05$ for groups with differential editing, Fig. 1H, I). Overall, at each target, we observed a range of editing efficiencies which differed depending on the deaminase, spanning from two-fold to four-fold differences in editing. The most efficient CBEs were TadCBEd, which successfully edited 75% of the targeted SAs (mean editing rate ~30%) followed by CBE4max (50%, mean editing rate ~40%), evoFERNY (50%, mean editing rate ~26%) and RrA3F (F130L) (50%, mean editing rate ~29%). SsAPOBEC3B (R54Q) and PpAPOBEC1 (H122A) only edited one and

https://doi.org/10.1038/s41467-024-54529-y

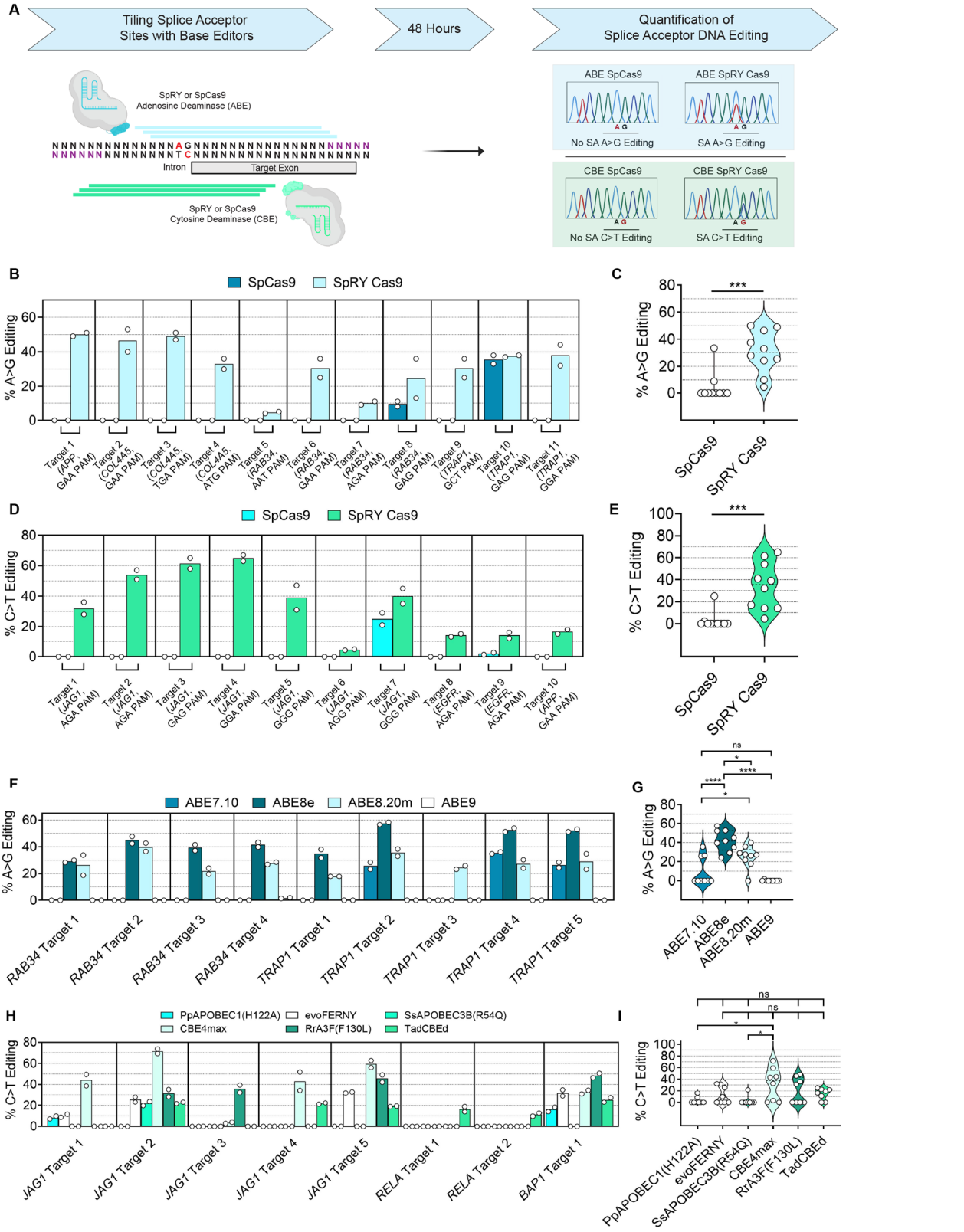

two target sites, respectively, at rates lower than 22% (Fig. 1H, I). Interestingly, TadCBE and RrA3F (F130L) enabled editing of target sequences that were resilient to modification by every other BE system tested (Fig. 1I).

Thus, fusion of SpRY Cas9 with different deaminases not only increased the number of exons that can be targeted but also enhanced editing efficiency at different SAs.

Simultaneous editing of SA and SD sites enhances exon-skipping

While there are different parameters that can influence exon splicing, including modifications at SA sites as we have previously shown[10], a simplistic model suggests that exon skipping rates are the result of the equilibrium between the DNA modification that disrupts different splicing elements that favor skipping, and the persistence of non-edited functional splicing elements that favors exon inclusion, such as

Fig. 1 | SpRY Cas9 in combination with different deaminases enables efficient disruption of targeted splice acceptors. A Schematic representation of the approach to disrupting splicing elements with near-PAMless ABEs (blue) or CBEs (green) by tiling eight sgRNAs per exon (Created in BioRender. Miskalis, A. (2024) https://BioRender.com/x92p416). Comparison of SpCas9 and SpRY Cas9 editing efficiency at the splice acceptors (SAs) of target exons using ABEs (**B**, **C**) or CBEs (**D**, **E**). Summary of editing efficiency at individual targets accomplished with SpCas9 or SpRY Cas9 ABEs (**C**) or CBEs (**E**). Comparison of DNA editing efficiency at multiple SAs using SpRY Cas9 fused with one of four different adenosine deaminases (**F**, **G**) or one of six different cytosine deaminases (**H**, **I**). Summary of editing efficiency at individual targets accomplished with different SpRY ABEs (**G**) or different SpRY CBEs (**I**). For (**F**–**I**), DNA editing rates were normalized to the protein expression of each deaminase from Fig. S1 by dividing each DNA editing rate by the normalized expression of each base editor. Values represent means and error bars indicate SD. For (**B**, **D**, **F**, and **H**), $n = 2$; $n = 10$ for (**C**); $n = 9$ for (**E**, **G**); $n = 8$ for (**I**). All replicates are biological replicates; ns, not significant; $^{*}p < 0.05$, $^{**}p < 0.01$; $^{***}p < 0.001$; two-tailed, unpaired t-test except for (**G**, **I**), which were analyzed via one-way ANOVA with Tukey's post hoc. Source data are provided as a Source Data file.

splicing enhancers or cryptic splicing elements. Thus, along with using SpRY Cas9 to edit SA sites, we reasoned that exon skipping could be enhanced by simultaneously targeting multiple splicing elements, such as SA and SD sites (Fig. 2A) and that this dual targeting could shift the equilibrium further towards exon skipping.

To test this hypothesis, we simultaneously targeted the SDs and SAs, referred to as dual splice site targeting, of four exons with SpRY-ABE8e or SpRY-CBE4max and used next-generation sequencing (NGS) to analyze splicing in HEK293T cells (Fig. 2B–D). At steady state, we did not detect alternative splicing at any of the targeted exons in control samples (Fig. S2A). Following treatment with ABEs, we observed that dual splice site targeting improved exon skipping compared to single splice site editing across all targets for multiple sets of sgRNAs (Figs. 2B, Figs. S2B, S2C, S3, Table S2), with effects ranging from synergistic (Fig. 2B) to additive (Fig. 2C). In scenarios such as targeting exon 12 of *JAG1*, exon skipping improved from undetectable and ~9% when targeting the individual SA or SD sites respectively, to 37% when both sites were edited simultaneously (SA 1/SD 1 vs SA 1, $p < 0.0001$, SA 1/SD 1 vs SD 1, $p < 0.0001$, Fig. 2B). Dual splice site targeting enhanced skipping even in cases where individually targeting the SA or SD sites had no effect, such as for *LMNA* exon 11, where skipping increased from undetectable for the SA an SD sites to 38% when targeting the SA and SD (SA 1/SD 1 vs SA 1, $p = 0.0001$, SA 1/SD 1 vs SD 1, $p < 0.0001$, Fig. 2B). When targeting *HSF1* exon 11, exon skipping improved from ~40% when targeting the SA alone to ~65% when both splice sites were mutated (SA 1/SD 1 vs SA 1, $p = 0.013$, SA 1/SD 1 vs SD 1, $p = 0.001$, Fig. 2C). When targeting *RELA* exon 7, the improvement in exon skipping was additive, increasing from ~33% and ~29% skipping when targeting the individual SA and SD sites respectively, to ~56% when targeted simultaneously (SA 1/SD 1 vs SA 1, $p = 0.031$, SA 1/SD 1 vs SD 1, $p = 0.014$, Fig. 2C).

Consistent with our findings for the ABEs, dual splice site targeting of SAs and SDs with CBEs improved skipping in 75% of all targeted exons, with the improvements found to vary in a similar manner to the ABEs (Fig. 2B–D, Fig. S2B, S2C, S3 Table S2). Like ABEs, synergistic and additive trends in exon skipping were observed for multiple sets of sgRNAs (Fig. S2B, S2C). For example, the improvement in exon skipping with CBEs was synergistic for both *EGFR* exon 23 (SA 1/SD 1 vs SA 1, $p < 0.0001$, SA 1/SD 1 vs SD 1, $p < 0.0001$, Fig. 2B) and *JAG1* exon 12 (SA 1/SD 1 vs SA 1, $p = 0.0003$, SA 1/SD 1 vs SD 1, $p = 0.0004$, Fig. 2B) when editing both the SA and SD, while the increase in exon skipping was additive for *BAP1* exon 2 (SA 1/SD 1 vs SA 1, $p = 0.0011$, SA 1/SD 1 vs SD 1, $p < 0.0001$, Fig. 2C). Finally, for *AHCY* exon 9, dual targeting did not improve exon skipping (SA 1/SD 1 vs SA 1, $p = 0.654$, SA 1/SD 1 vs SD 1, $p = 0.233$, Fig. 2D).

Additionally, when comparing the DNA editing rates between single and dual splice site targeting, there was no statistically significant difference amongst groups, except for editing at both the SA and SD for *JAG1* exon 12 CBEs (SA DNA editing of SA 1 vs SA 1/SD 1, $p = 0.0002$, SD DNA editing of SD 1 vs SA 1/SD 1, $p = 0.0006$, Fig. 2B). Here, DNA editing is reduced by ~50% at the SA and SD sites when simultaneously editing both splice sites compared with editing the sites individually. Despite the lower editing rates in DNA, exon skipping was drastically improved following dual splice site targeting, indicating the crucial importance of disrupting both SAs and SDs for skipping certain exons.

These results highlight that simultaneous targeting of multiple splicing sequences with SPLICER enhances full exon skipping outcomes.

SPLICER lowers cryptic splicing and intron retention

One problem frequently observed when inducing exon skipping is the induction of splicing aberrations, such as cryptic splicing and intron retention. Cryptic splicing can occur when the spliceosome machinery utilizes sites that closely resemble the canonical SA or SD sequences, resulting in a transcript in which the target exon is not fully skipped[13,38,46]. Similarly, intron retention can occur when disruption of a SA or SD does not induce full exon skipping; instead, part of an intron or the entire intron is incorporated into the mature mRNA[13,22,47]. While events such as these are complex and not fully understood, 'AG' and 'GT' bases near the consensus SD and SAs are frequently interpreted by the spliceosome machinery as cryptic SAs or SDs[13,47–49], respectively (Fig. 3), which can prevent full skipping of an exon when only one splicing element is disrupted.

Given our findings indicating that editing of both SA and SD sites can increase full exon skipping, we hypothesized that one reason for the increase in full-length exon splicing could be a decrease in the rate of cryptic splicing events that occur. In the case of alternative splicing patterns in *LMNA* exon 11, we observed that editing the SD alone induced an alternative splicing event, where a 'GT' dinucleotide that is normally part of the codon corresponding to residue V607 was recognized as a cryptic SD (Fig. 3A) and utilization of this sequence led to partial exon skipping that created a new reading frame for *LMNA* at a rate of ~53%. However, when editing the SA and SD simultaneously, the cryptic splicing isoform was reduced ~3-fold, and the entire exon was skipped at a rate of ~37% (SA 1/SD 1 vs SD 1, $p = 0.0001$, Fig. 3A), thus indicating that dual splice site targeting can reduce the recognition of a cryptic splice site, leading to an increased rate of full exon skipping. We also observed cryptic splicing caused by modifying the SA for *HSF1* exon 11 (Fig. 3B). In this instance, a cryptic 'AG' sequence present at S419 acted as a cryptic SA, leading to a frameshifted transcript with a premature termination codon (PTC) within exon 11. This cryptic splicing event was reduced ~10-fold upon simultaneous splice site disruption (SA 1/ SD 1 vs SA 1, $p = 0.0005$, Fig. 3B).

Additionally, when only editing the SD in *HSF1* exon 11, there exists a cryptic SD created by a 'GT' motif located at the serine residue directly before the canonical SD, which can be used as a splice site whose utilization leads to a frameshift that extends through exons 12 and 13 and results in a premature stop codon at residue 492 of exon 13. When targeting the SD of *HSF1* exon 11, the cryptic SD event was recognized in ~4.8% of cases. This cryptic event was reduced by ~4.9-fold to 0.97% for dual splice site targeting (SA 1/ SD 1 vs SD 1, $p < 0.0001$, Fig. S4A).

To further demonstrate the ability of SPLICER to mitigate aberrant cryptic splicing, we targeted the SA of *BAP1* exon 2 with CBE4max, where the full exon skipping rate was ~49% and a partial exon 2 skipping event, which stems from a cryptic SA, was ~42% (Fig. 3C). Dual splice site targeting decreased cryptic splicing by ~39% (SA 1/SD 1 vs SA 1,

https://doi.org/10.1038/s41467-024-54529-y

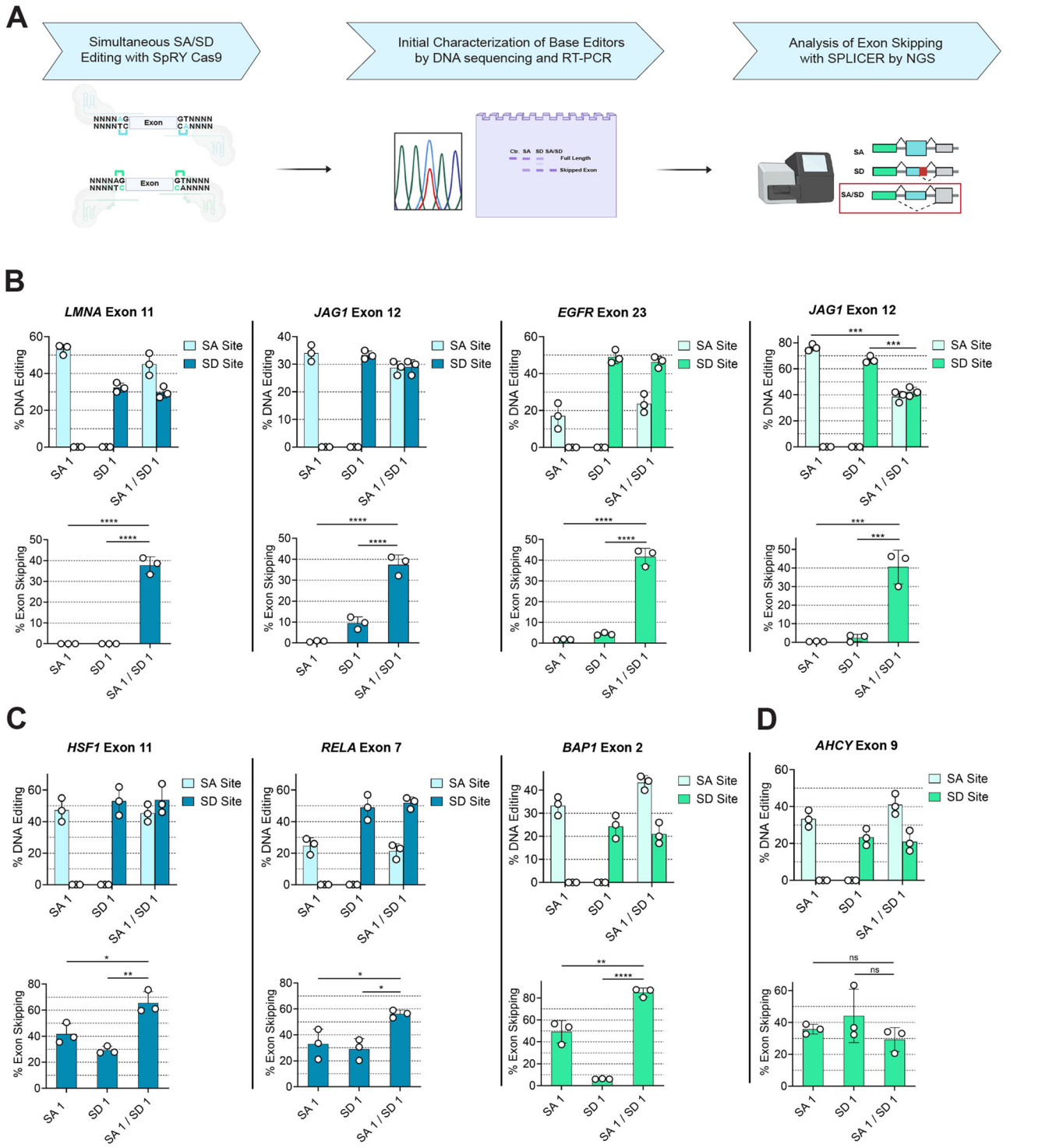

Fig. 2 | Simultaneous editing of splice sites with SPLICER enhances exon skipping. A Illustration of SPLICER strategy for simultaneously targeting SAs and SDs with ABEs or CBEs followed by screening to identify effective BE systems and characterization next-generation sequencing (Created in BioRender. Miskalis, A. (2024) https://BioRender.com/x43x713). **B**–**D** Editing of AG dinucleotides in the SA (top panel) and GT dinucleotides in the SD (medium panel) and exon skipping (bottom panel) with ABEs (highlighted blue) or CBEs (highlighted green). Improvements in exon skipping were synergistic when targeting *LMNA* exon 11, *EGFR* exon 23 and *JAG1* exon 12 (**B**). Improvements in exon skipping were additive when targeting *HSF1* exon 11 and *RELA* exon 7 (**C**). Editing of SA and SD of *AHCY* exon 9 with ABEs did not improve exon skipping rates compared with editing of SA or SD alone (**D**). All measurements of full-length exon skipping were performed by NGS except for *LMNA* exon 11, which were measured via Sanger Sequencing. Values represent means and error bars indicate SD. All replicates are biological replicates originating from three independent transfections of each sgRNA set; $n = 3$ for all experiments; ns, not significant; $^{*}p < 0.05$; $^{**}p < 0.01$; $^{****}p < 0.0001$; one-way ANOVA, Tukey's post hoc comparing SA/SD to SA and SD except for the comparison showing the DNA editing rates for *JAG1* exon 12, which was performed via a two-tailed, unpaired *t* test. Source data are provided as a Source Data file.

https://doi.org/10.1038/s41467-024-54529-y

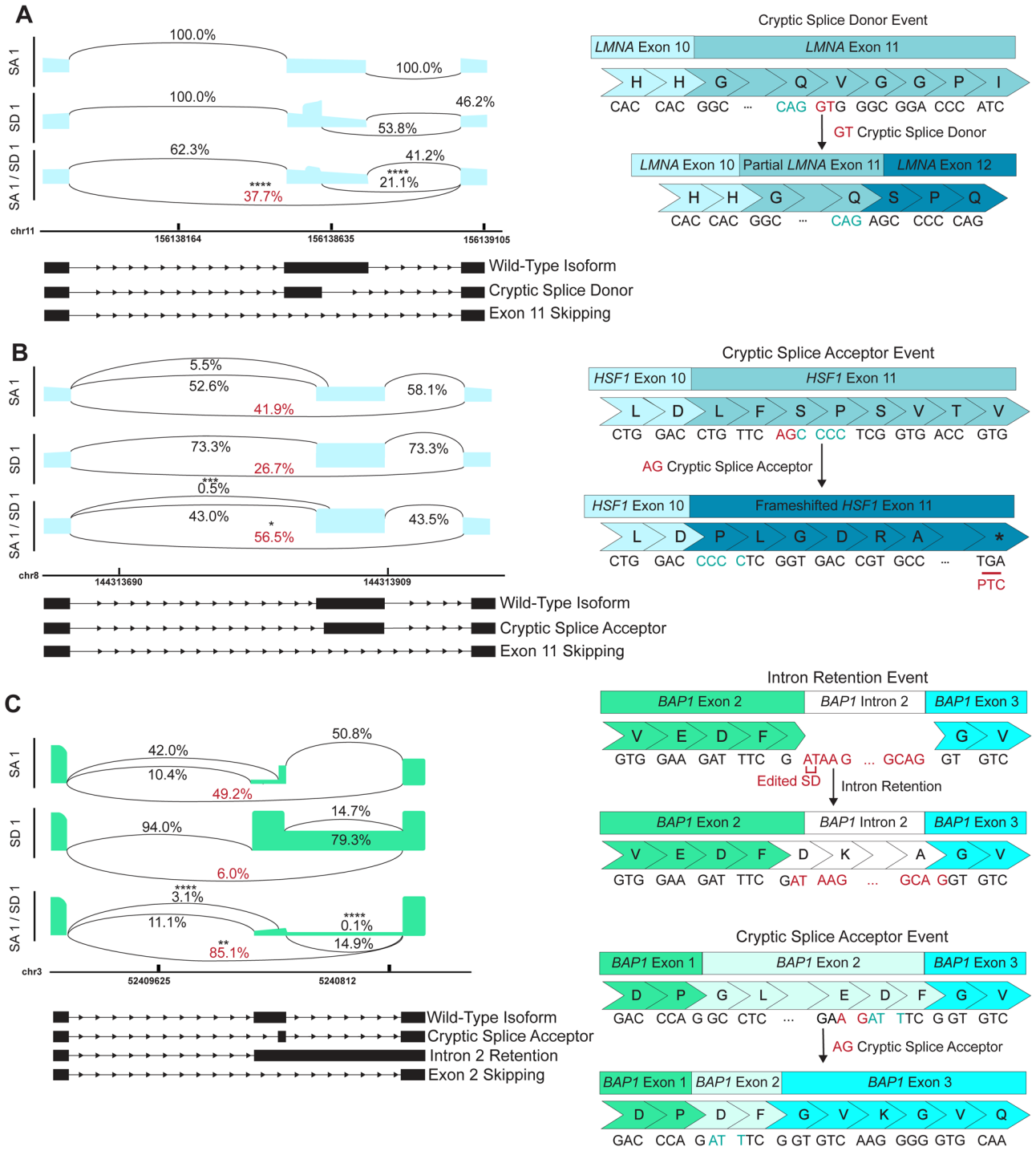

Fig. 3 | SPLICER improves exon skipping through reduction of Both cryptic splicing and intron retention. A Sashimi plot describing exon splicing following ABE editing of *LMNA* exon 11 with SPLICER, in which a cryptic SD site is recognized in the middle of the exon when editing the SD (left), leading to no exon skipping and partial retention of exon 11 (right). This aberrant splicing event is reduced 3-fold by ABE editing of both SA and SD sites. **B** Sashimi plot representing splicing of *HSF1* exon 11 before and after ABE editing of splicing elements demonstrating a cryptic SA recognized in *HSF1* exon 11 (left). This cryptic splicing leads to a frameshift mutation in a protein, which results in a premature termination codon in exon 11 (right). Cryptic splicing is reduced 10-fold when editing both sites (left). **C** Sashimi plot describing splicing of *BAP1* exon 2 following editing with CBEs (left). Cryptic splicing and intron retention occur with SA and SD editing alone, leaving an in-frame, but mutated protein (right). Both events are minimized with SPLICER (left). All measurements of full and cryptic exon skipping were performed by NGS except for *LMNA* exon 11, in which full exon skipping was measured by RT-PCR densitometry. For sashimi plots, values represent the mean. All replicates are biological replicates originating from three independent transfections of each sgRNA set; $n = 3$ for all experiments; $^{*}p < 0.05$; $^{**}p < 0.01$; $^{***}p < 0.001$; $^{****}p < 0.0001$; one-way ANOVA, Tukey's post hoc comparing cryptic splicing events in SA or SD to the rate of that cryptic splicing event in simultaneous SA/SD editing. Source data are provided as a Source Data file.

$p = 0.0003$, Fig. 3C) and increased full-length exon skipping by ~36% (SA 1/SD 1 vs SA 1, $p = 0.0011$, Fig. 3C).

In addition to reducing unwanted cryptic splicing, we also observed that SPLICER decreases intron retention events. For example, when targeting the SD of *BAP1* exon 2, full exon skipping was only detected in ~6% of the transcripts, while ~79% of the transcripts retained intron 2 fully. This aberration was minimized by targeting both SD and SA sequences, which reduced intron retention to <1% (SA 1/SD 1 vs SD 1, $p < 0.0001$, Fig. 3C) and improved full exon skipping to 85%.

Lastly, along with aberrant splicing, another possible adverse event resulting from exon skipping with base editors is mRNA mutations that occurs due to bystander DNA editing, which could lead to mutated proteins when the exon is not skipped or the intron is retained (Fig. S4B). Analysis of the genomic DNA from the 7 genes targeted in Fig. 2 revealed that three genes had exonic or intronic bystander DNA editing that could potentially lead to mutations in mRNA, including *HSF1* exon 11 and *JAG1* exon 12 when targeted with ABEs and *BAP1* exon 2 when targeted with CBEs (Figs. S5, S6). We observed that targeting only the SD of *HSF1* exon 11 introduced a mutation in mRNA at the last base of the exon at a rate of 0.6%. This mRNA editing was not detected in samples targeted by dual splice site base editing. When targeting *JAG1* exon 12, no mRNA editing was detected for either single or dual splice site editing despite the presence of bystander mutations within the exon and a low rate of exon skipping when only editing the SD. When targeting *BAP1* exon 2, which retains intron 2 at ~79% by editing only the SD, all reads containing the retained intron also had the sequence of the mutated splice donor (Fig. S4B). The frequency of this mutation was drastically reduced by targeting both splice sites (SD vs SA/SD, $p < 0.0001$, Fig. S4B).

These results support that SPLICER improves the efficiency and precision of full exon skipping through the reduction of aberrant splicing events.

SPLICER reduces in vitro Aβ42 production and skips APP exon 17 in vivo

Given the efficiency of exon skipping accomplished with SPLICER, we next sought to determine whether it could be utilized to skip exons with therapeutic value, such as exon 17 in the *APP* gene, which is resilient to skipping with CRISPR-SKIP. *APP* is located in chromosome 21 and encodes the amyloid β precursor protein (Fig. 4A)[24,25]. APP digestion by β- and γ- secretase generates the Aβ42 peptide, which is hypothesized to contribute to the pathogenesis of Alzheimer's disease (AD)[24,50]. Importantly, this cleavage site is encoded within exon 17, an exon whose skipping has been previously shown to reduce the formation of Aβ42 plaques[25,51].

Using SpRY Cas9, we tiled the SA and SD sites of *APP* exon 17 and identified one sgRNA that edited the SA of exon 17 with SpRY-ABE8e (50%) and one with SpRY-CBE4max (16%) in HEK293T cells (Fig. 4B). We were unable to identify sgRNAs that edited the SA with SpCas9 (Fig. 4B), and since SpRY-ABE8e edited the SA with higher efficiency than CBE4max, SpRY-ABE8e was used for further experiments. For targeting the SD, we identified three sgRNAs with SpRY-ABE8e that edited the splice site with efficiencies of 78%, 67%, and 16% (labeled SD 1, SD 2, and SD 3, respectively) (Fig. 4C, D). In addition to editing the canonical SD, we identified two additional bystander 'GT' motifs that were edited with these sgRNAs, one within the exon at amino acid residue V736 and another in intron 17 four bases after the canonical SD (Fig. 4D). Next, we sought to determine if the cryptic 'GT' and canonical SD editing occurred simultaneously (Fig. S7A–C) and we observed that for SD 1 sgRNA, the SD and intronic cryptic 'GT' sequence were edited simultaneously in 91% of instances, with editing occurring only at one site in 4.5% of the instances for both the intronic 'GT' and the canonical SD (Fig. S7A). For the SD 2 sgRNA, approximately 50% of DNA with A > G editing showed simultaneous exonic bystander and SD editing, while the other 50% only contained SD DNA editing (Fig. S7B). For SD 3 sgRNA, we observed that in 60% of the edited DNA sequences only the intronic 'GT' site was modified, while 29% contained both intronic 'GT' and canonical SD editing (Fig. S7C). Dual splice site editing increased the rate of intronic 'GT' editing to ~97%. Thus, each SD sgRNA showed unique characteristics for simultaneously editing the canonical SD and bystander sites, which may influence exon skipping and cryptic splice site recognition.

When analyzing exon skipping rates, despite the high rates of editing observed at the SA site for *APP* exon 17, we observed limited skipping (~0.9%) when targeting the SA alone (Fig. 4E). However, when the SA was targeted in combination with one of three different SD-targeting sgRNAs described above, NGS analysis showed exon skipping in pooled HEK293T cells at rates of ~74%, ~22%, and ~25%, respectively (Fig. 4E). With all sgRNAs, targeting the SA and SD sites improved full-length exon skipping rates compared to single splice site targeting, ranging from a small increase to a synergistic improvement (69% to 74% for SA/SD 1, 6.5% to 24% for SA/SD 2, 15% to 27% for SA/SD 3, $p < 0.05$ for all, Fig. 4E). Additionally, we found that splice site editing did not significantly ($p > 0.05$) affect *APP* mRNA expression measured by qPCR in 293T cells. (Fig. 4F).

Notably, when characterizing the precision of the splicing events following editing of *APP* exon 17, we observed that simultaneous targeting of both the SA and SD again reduced cryptic splicing events (Fig. 4G, H). For example, when the SA was targeted individually, a cryptic 'AG' motif located between A692 and E693 was utilized for splicing, leading to a premature termination codon within exon 17 in ~7% of transcripts, an outcome that was almost completely abolished with dual splice site-editing (SA/SD 1 vs SA, $p < 0.0001$, Fig. 4G). When editing the canonical SD with the sgRNA SD 2, a partial intron retention event, whereby a cryptic intron SD was utilized, occurred in 39% of transcripts. This aberrant splicing was reduced by over 50% with simultaneous editing of the SD and SA (SA/SD 2 vs SD 2, $p = 0.0004$, Fig. 4H), demonstrating the ability for dual splice site targeting to reduce unwanted cryptic splicing.

Since we had previously observed that DNA editing in coding regions can lead to mutations in mRNA transcripts that can be reduced with dual splice site targeting, we analyzed mutations in the mRNA of APP exon 17 and we observed that sgRNAs SD 1 and SD 3 did not introduce mutations detectable in mRNA. However, SD 2 sgRNA installed mutations that were detected in mRNA as a result of a bystander editing in exon 17 (Fig. S7D-E). The frequency of these mutations was reduced by dual splice site editing by two-fold (SD 2 vs SA/SD 2, $p = 0.002$, Fig. S7D). Approximately 2% of transcripts with mRNA mutations occur in mRNA containing the normal exon 17–18 splice junctions, and this specific event is reduced three-fold with simultaneous SA and SD editing SD 2 vs SA/SD 2, $p = 0.003$, Fig. S7F). These results emphasize the potential for SPLICER to reduce mRNA mutations. For subsequent experiments, we used the SA sgRNA in combination with the SD 1 sgRNA as it possessed the highest exon skipping without creating undesired mRNA mutations.

Furthermore, we characterized off-target DNA editing and the effect of splice site editing on the transcriptome. To measure the off-target DNA activity of our *APP* sgRNA set, we analyzed editing at five potential off-target sites, which we identified by Cas-OFFinder[52]. This analysis revealed no appreciable A-to-G editing at any predicted site compared to control HEK293T cells ($p > 0.05$, Fig. S8A, B). To determine if our dual-splice site editing platform influenced overall RNA expression on a transcriptome-wide scale, we performed RNA-seq and differential gene expression (DGE) analysis following targeting of *APP*exon 17[53]. This analysis revealed increased expression of only 3 genes, *HSPA6*, *ZCCHCH12*, and *RPL21P120* (Benjamini-Hochberg adjusted $p < 0.05$, Fig. S8C). No genes were found to be down-regulated. Additionally, we analyzed gene expression pathways

https://doi.org/10.1038/s41467-024-54529-y

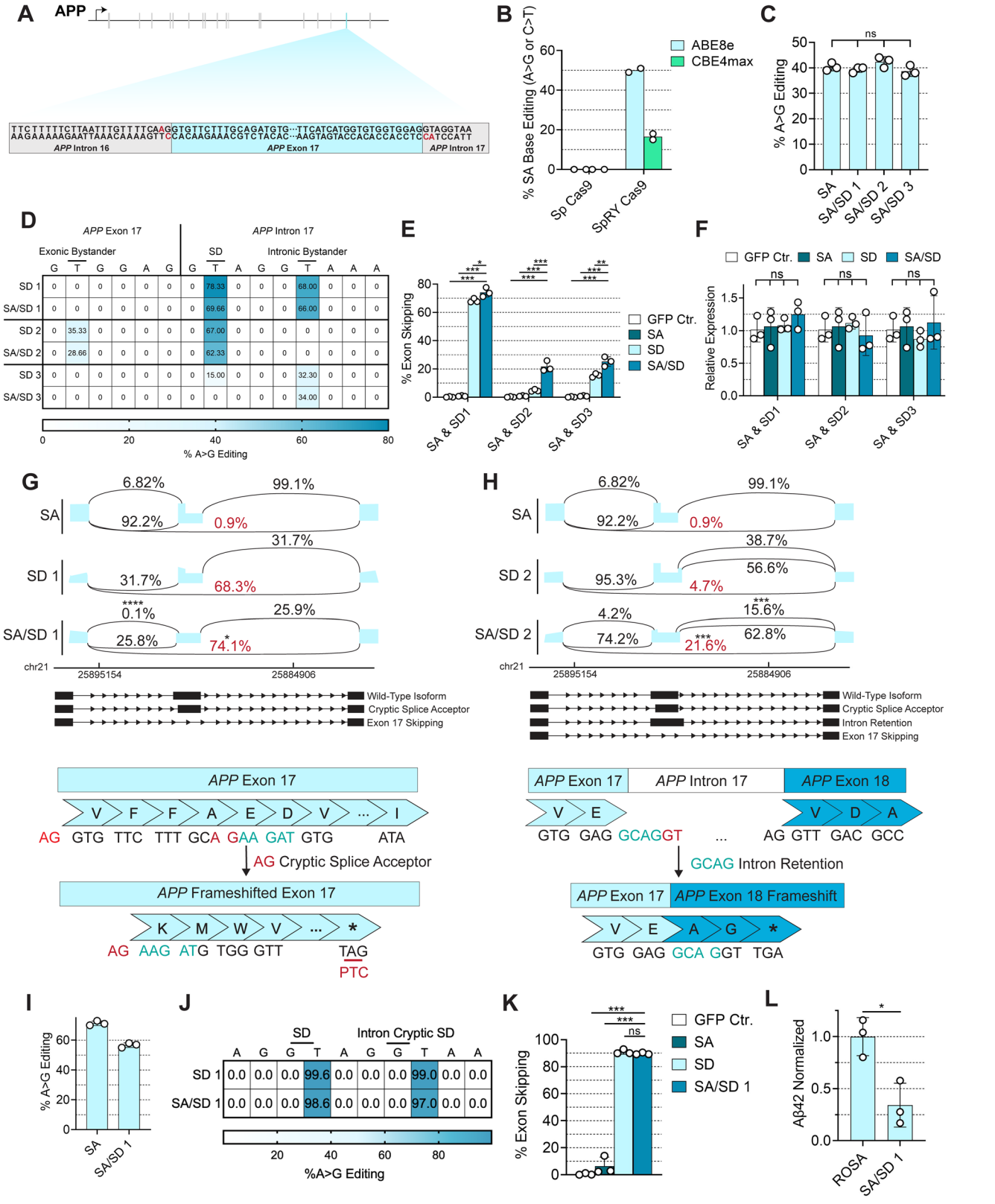

associated with mismatch repair (KEGG pathway hsa03430) and base excision repair (KEGG pathway hsa03410) and observed no changes in pathway expression for any genes when compared to control cells ($p > 0.05$, S8D, E, G, H). When analyzing the transcriptomic profile for genes linked with AD (KEGG pathway hsa05010), we found no change in expression associated with pathways implicated in the pathogenesis of AD, including *APP* (Fig. S8F, I), further demonstrating that simultaneous SA/SD targeting does not induce misregulation of gene expression.

Next, we determined whether dual splice site-targeting of *APP* exon 17 using SA/SD could influence the formation of Aβ42 in BE(2)-M17 cells, which are commonly used to model aspects of AD as they produce high levels of the Aβ42 peptide[54]. Following enrichment of transfected cells, we measured editing efficiencies of ~60% at the SA

Fig. 4 | SPLICER Skips APP Exon 17 in vitro and Reduces Production of Aβ42. **A** Schematic representation of *APP* and sequence of *APP* exon 17 and introns 16 and 17. **B** Genomic DNA editing rates at the SA of *APP* exon 17 with ABE8e and CBE4max fused with SpCas9 or SpRY Cas9 in HEK293T cells. **C** SA DNA editing rates with SpRY Cas9 ABE8e when editing the SA alone or in combination with a panel of sgRNAs targeting the SD. **D** SD DNA editing rates with sgRNAs targeting the SD alone or in combination with a sgRNA targeting the SA. Editing at the canonical and cryptic SDs is highlighted. **E** *APP* exon 17 exon skipping rates with an sgRNA targeting the SA in combination with one of 3 different sgRNAs targeting the SD measured by NGS. **F** qPCR quantification of total *APP* mRNA. **G**, **H** Quantification of *APP* exon 17 exon splicing (top) and schematic representation of the corresponding splicing event (bottom) following targeting of the SA with a sgRNA and SD with two different sgRNAs. (**I**) DNA editing at the SA and (**J**) SD of *APP* exon 17 in BE(2)-M17 neuroblastoma cells following enrichment with puromycin. **K** Exon skipping rates for *APP* exon 17 in puromycin selected BE(2)-M17 neuroblastoma cells. **L** Aβ42 levels in BE(2)-M17 cells following skipping of *APP* exon 17 in comparison with control cells using ELISA. All measurements of full-length and cryptic exon skipping were performed by NGS while all DNA editing rates were measured via Sanger sequencing. For all bar graphs, values represent means and error bars indicate SD. For heatmaps, values represent means. For sashimi plots, values represent means. In experiments performed in HEK293 cells, each replicate is a biological replicate originating from an independent transfection of each sgRNA. In experiments with BE(2)-M17 cells, a single transfection was performed with each sgRNA set to generate a puromycin selected cell line. Following cell line generation, each sgRNA set was maintained amongst three separate plates with each replicate deriving from one plate; $n = 3$ for all experiments; ns, not significant; $^{*}p < 0.05$; $^{**}p < 0.01$; $^{***}p < 0.001$; one-way ANOVA, Tukey's post hoc comparing SA/SD to SA and SD except for (**B**, **L**), which were analyzed via a two-tailed, unpaired t-test. Source data are provided as a Source Data file.

site and editing efficiencies >99% at both the canonical SD and the cryptic intron SD (Fig. 4I, J). NGS analysis of mRNA revealed ~90% exon skipping upon simultaneous targeting of the SA and SD sites (Fig. 4K). Like our findings in HEK293T cells, when editing the SA alone, a cryptic 'AG' splice acceptor motif was found to be recognized within amino acids V692 and E693 at a rate of 21%. We found that usage of this cryptic splicing was reduced to <1% when editing both the SA and SD ($p < 0.0001$, Fig. S9A), with no other alternative splicing event observed (Fig. S9A). Additionally, to confirm that SPLICER effectively skipped *APP* exon 17 and did not generate unexpected alternatively spliced isoforms, we performed RT-PCR with primers designed to amplify *APP* exons 1 to 18 (Fig. S9B). In wild-type cells we observed a single product corresponding to the canonical full-length *APP* mRNA and no alternatively spliced products were detected. Following targeting of *APP* exon 17 with SPLICER we also observed a single product but, in this case, corresponding to an *APP* isoform lacking exon 17. No other splicing event was detected thus supporting that SPLICER did not stimulate aberrant splicing (Fig. S9B).

Lastly, using ELISA, we quantified the production of Aβ42 in BE(2)-M17 cells and we observed a ~70% decrease of Aβ42 peptide following dual splice site targeting (SA/SD vs Rosa26, $p = 0.015$, Fig. 4L).

To further validate the potential of SPLICER, we sought to induce skipping of *APP* exon 17 in a mouse model of AD, specifically $APP^{K670N/M671L}$ mice (R1.40)[55]. These are C57/BL6 mice which harbor a yeast artificial chromosome expressing the full human *APP* gene with two known familial mutations associated with AD, K670N and M671L. Importantly, these mice contain the entire human *APP* gene, including introns, an element not typically featured in other mouse models of AD, and necessary for testing exon skipping strategies. To deliver our BE in vivo, we utilized adeno-associated virus (AAV), specifically AAVrh10, which can efficiently transduce the hippocampus[29,30,53,56], an area of the brain typically affected in AD by the formation of Aβ42 plaques. However, as the size of a full-length BE exceeds the ~4.7 kilobase (kb) packaging capacity of an AAV vector genome, we employed a split-intein platform[57] that enables delivery of a BE from two AAV vectors. In this system, the BE is split into two halves at amino acid 712 of the SpRY Cas9 protein, with its resulting N- and C-termini fused to the N- and C-intein fragments from the DnaB protein of *Rhodothermus marinus*. Upon their co-expression, these two inteins dimerize and self-excise, which we found leads to the reconstitution of the full-length BE protein.

We injected AAVrh10 vectors encoding either our *APP*-targeting split-intein BE platform and EGFP-KASH[58], with the expression of each driven by a CAG promoter, to the hippocampus of four- to seven-week-old R1.40 mice (Fig. 5A). At one-month post-injection, we used fluorescence-activated cell sorting (FACS) to measure the transduction efficiency within the hippocampus, finding that ~23% of sorted cells were positive for EGFP-KASH (Fig. S10A). Using NGS, we next analyzed DNA editing within bulk hippocampal tissue from the injected mice and we determine that the editing efficiency was ~6.4% at the SA (Fig. 5B), ~22.4% at the SD, and ~23.4% at the cryptic SD (Fig. 5C). Of note, however, we found that these editing rates were approximately three-fold higher within the FACS sorted nuclei (Fig. S10B, C). Last, using NGS, we assessed the frequency of *APP* exon 17 skipping in mRNA from bulk hippocampal tissue of injected mice, finding that mice treated with the *APP* targeting split-intein BE platform had a ~20% exon 17 skipping (SA/SD vs mRosa26, $p = 0.003$, Fig. 5D), with our deep sequencing analysis further revealing no aberrant cryptic splicing from SA/SD 1 DNA editing, altogether indicating that SPLICER achieved precise, full exon 17 skipping in vivo (Fig. 5E).

In conclusion, we have developed SPLICER, a method that increases the efficiency and precision of exon skipping by CRISPR base editors. We demonstrate the potential of SPLICER by targeting a high-value target for AD in a mouse model of the disorder.

Discussion

In this work we developed SPLICER, a platform for exon skipping with base editors that overcomes the limitations of previously described technologies. This platform utilizes base editors with relaxed PAM requirements fused with different deaminases that, when targeted to both SDs and SAs simultaneously, increase exon skipping efficiency and decrease splicing aberrations.

Potential applications of SPLICER include therapeutic exon skipping to restore protein expression[11,59–62], disruption of splicing sequences to interrogate and dissect exon splicing, gene knock out by altering the reading frame through exon skipping[15,63] or massively parallel loss-of-function screens[64], which also take advantage of gene knock out by shifting the reading frame.

SPLICER provides significant advantages over other methods for exon skipping such as ASOs, which are currently used as gene therapies for treating Duchene muscular dystrophy[65,66] or retinitis pigmentosa[67,68], because the transient nature and rapid clearance of ASO requires repeated administration and provides only a temporary benefit with limited activity in the periods of time leading to the new dosage. The permanent nature of the modifications introduced in genomic DNA by base editors is advantageous, although the transient effects of ASOs are reversible, which could be beneficial if adverse effects occur.

Other gene editing technologies, such as traditional CRISPR-Cas9 nucleases[69,70] or prime editors[71,72], can also be used to disrupt splicing sequences. However, as the knowledge about the potential deleterious effects of DSBs increases, it becomes critical to utilize technologies that minimize DSBs and induce minimal genotoxicity, which can make base editors preferable over nucleases or prime editors[1,73,74].

One limitation of base editors is their propensity to introduce bystander mutations, which could hinder therapeutic applications that require precise correction of a single base mutation[75]. Importantly, we have observed that while intronic bystander edits do not directly

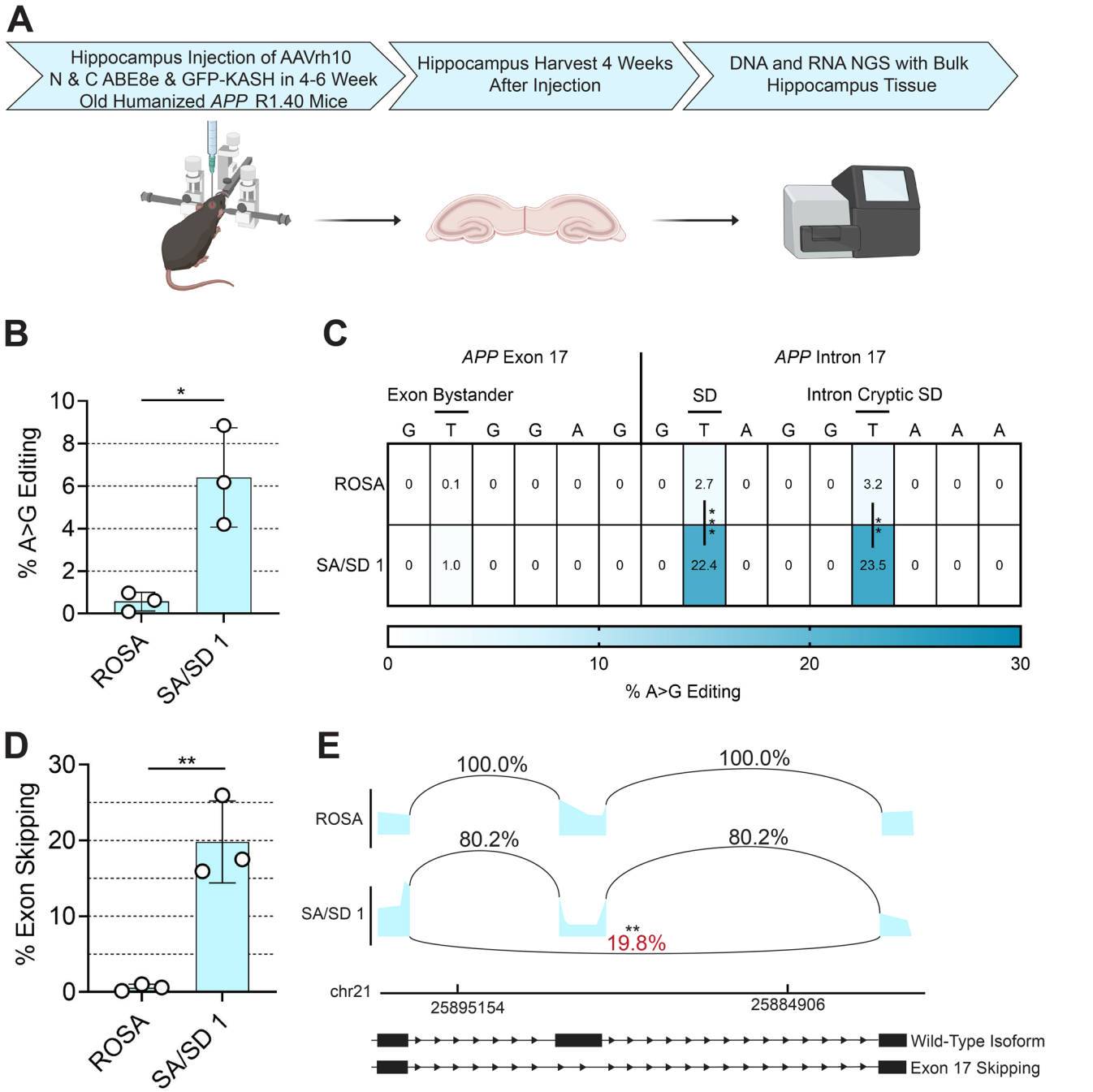

Fig. 5 | SPLICER enables efficient DNA editing and full exon skipping in a humanized mouse model of Alzheimer's Disease. A Experimental workflow of in vivo editing following AAVrh10 injection of BEs targeting the SA and SD of *APP* exon 17 in the hippocampus of R1.40 mice (Created in BioRender. Miskalis, A. (2024) https://BioRender.com/f96o812). **B** In vivo genomic DNA editing of *APP* exon 17 SA and (**C**) SD in bulk hippocampus tissue measured using NGS. **D** In vivo exon skipping of *APP* exon 17 in bulk hippocampus tissue following treatment with BEs targeting the SA and SD. **E** Sashimi plot of splicing events in control mice and mice injected with BEs targeting the SA and SD of *APP* exon 17. For all bar graphs, values represent means and error bars indicate SD. For heatmaps, values represent means. For sashimi plots, values represent means. Each replicate value is from the hippocampus of an individual mouse. All measurements of exon skipping were performed by NGS and all DNA editing rates were measured by NGS. $n = 3$ for all groups; $^{*}p < 0.05$; $^{**}p < 0.01$; two-tailed, unpaired t-test. Source data are provided as a Source Data file.

create mutations that will be included in mRNA transcripts, they can modify splicing regulatory elements such as splice silencers or enhancers and generate aberrant transcripts. Therefore, extensive characterization of base editing profiles is crucial to accomplish efficient exon skipping.

Guide-dependent and guide-independent off-target effects are important concerns when using base editors[76,77]. Since SPLICER targets sequences that are conserved in the genome, it is possible that the sgRNAs utilized may be at a higher risk for off-target effects. Although we did not observe any off-target mutations at ten computationally predicted off-target sites for the sgRNAs targeting *APP* exon 17, this analysis of off-target effects was limited and only measured ten predicted off-target sites. Further analysis using unbiased methods for detecting off-target mutations such as EndoV-seq[78] will be needed to get a more comprehensive view of off-target effects for dual splice site editing for *APP* exon 17. Guide-independent off-target effects are

derived from the nucleic acid binding capability of the deaminases and occur more frequently when using CBE than ABEs[77,79,80]. While newer generations of highly specific CBEs have been developed[40–42], we generally utilize ABEs whenever possible, which is advantageous not only because of their higher editing activity but also their specificity. Importantly, a CBE was recently developed from ABEs[42], which has improved specificity and has proven to be effective for inducing exon skipping in our work.

SPLICER was not sufficient to accomplish skipping of all targeted exons (Fig. 2). One possibility for the lack of improved exon skipping at exon 9 of AHCY is the presence of exon splice enhancer (ESE) sequences, which bind to Ser/Arg rich (SR) proteins that recruit spliceosome proteins[81,82]. We studied the presence of ESE utilizing ESEfinder[82] and determined that, within AHCY exon 9, there are motifs predicted to function as splice enhancers (high affinity to SF2/ASF: score 3.76, SC35: score 3.69, SC35: score 4.14, SRp40: score 3.88, SRP55, score 4.69)[82], which may explain why this particular exon appeared resistant to improved exon skipping with dual splice site editing. Interestingly, Qiu and coworkers have recently shown that ESE can be targeted with BEs to accomplish exon skipping[83]. While their results are intriguing, the approach has high potential to introduce exonic mutations without accomplishing exon skipping, which could lead to adverse effects.

One important caveat of our analysis is that we performed targeted PCR in combination with NGS to study skipping outcomes. In instances in which the outcome is a frame shift followed by nonsense mediated decay it is likely that the mRNA is degraded too quickly to be detected using our approach. Similarly, in cases of intron retention where the amplicon is too large to be detected by the chosen PCR primers, it is likely that our approach failed, resulting in underestimation of this splicing outcome. Future studies utilizing long-read analysis will be needed to further improve our understanding of exon skipping.

Lastly, we show the application of SPLICER for skipping *APP* exon 17, an approach with potential therapeutic value in Alzheimer's disease. By skipping exon 17, the binding site for some secretases is lost and generation of Aβ42 decreases. Previous attempts to skip this exon with BEs had been unsuccessful despite high editing rates at the SA and the lack of tools for targeting additional splice sites prevented further optimization of the approach. Using SPLICER, we have identified multiple sgRNAs with different editing profiles that have contributed to our understanding of the splicing events governing this transcript. We observed that editing the canonical SD activates a cryptic SD that prevents exon skipping and only when simultaneously editing both the canonical SD and cryptic SD sites with SPLICER we were able to effectively induce exon skipping. Additionally, *APP* exon 17 skipping was further enhanced by the simultaneous disruption of the SA, an event that reduced Aβ42 production in vitro. SPLICER had no effect on *APP* mRNA levels of expression, as determined by qPCR, however, RNA-seq did reveal that *APP* exon 17 disruption affected the expression of the genes *HSPA6*, *ZCCHCH12*, and *RPL21P120*.

Critically, SPLICER functions efficiently in vivo for targeting *APP* exon 17, accomplishing 20% exon skipping in a humanized *APP* mouse model when delivered by AAVrh10. While the skipping rate in vivo was approximately three-fold lower than the observed in vitro efficiency, when taking into consideration the in vivo transduction efficiency, which we measured as ~23.6%, this result emphasizes the potential of the approach, which we anticipate could be further improved following optimization of delivery.

In summary, we report the development of the SPLICER toolbox, which enables enhanced targeting of exons and improves the precision of exon skipping by reducing cryptic splicing via simultaneous editing of multiple splicing elements. We demonstrate the in vivo applicability of SPLICER in a humanized mouse model of Alzheimer's disease and anticipate that this technique will enable a broad range of applications.

Methods

Ethics statement

All animal procedures were approved by the Institutional Animal Care and Use Committee at the University of Illinois and conducted in accordance with the National Institutes of Health (NIH) Guide for the Care and Use of Laboratory Animals.

Plasmids and cloning

The plasmid encoding the U6-sgRNA expression cassette was obtained from Addgene (#47108). The full-length -CBE4max construct was purchased from Addgene (Plasmid #139999). The full-length SpRY-ABE8e plasmid was generated through Gibson Assembly of gBlock Gene Fragments (Integrated DNA Technologies) containing the adenosine deaminase in Addgene Plasmid #138489 and the SpRY-CBE4max backbone. To build the ABE and CBE constructs consisting of different deaminases described in Fig. 1, first SpRY mutations were cloned via Gibson Assembly of gBlock Gene Fragments (Integrated DNA Technologies) into split BE-expressing plasmids described in our previous work[18,57]. Then, different deaminases were cloned into the plasmids via Gibson Assembly of gBlock Gene Fragments. For experiments in BE(2)-M17 cells, which utilized a plasmid encoding SpRY-ABE8e-T2A-Puro, SpRY mutations, ABE8e deaminase, and the puromycin resistance gene were cloned via Gibson Assembly of gBlock Gene Fragments into the lentiviral expression plasmid pLenti-EFS-FNLS-P2A-BlastR[11]. Plasmids encoding the split AAV SpRY-ABE8e constructs were cloned via Gibson Assembly of gBlock Gene Fragments into our previously described AAV split Cas9 BE3 plasmids to insert SpRY mutations as well as to replace APOBEC1 with ABE8e[57]. All amino acid sequences from these plasmid constructs are provided in Table S1.

All oligonucleotides used in this work were obtained from Integrated DNA Technologies. The oligonucleotides for sgRNA generation were hybridized, phosphorylated and cloned following the U6 sgRNA vector using BbsI, Bsa1, of BsmBI sites with sequences are provided in Table S2.

New constructs will be made available through the Addgene plasmid repository.

Cell culture and transfections

The cell line HEK293T was obtained from the American Type Culture Collection (ATCC; catalog number CRL-3216) and was maintained in DMEM supplemented with 10% fetal bovine serum and 1% penicillin/streptomycin at 37 °C with 5% CO_2. BE(2)-M17 cells were obtained from the ATCC (CRL-2267) and maintained in 1:1 EMEM:Ham's F12K supplemented with 10% fetal bovine serum and 1% penicillin/streptomycin at 37 °C with 5% CO_2.

HEK293T cells were transfected in 24-well plates with Lipofectamine 2000 (Invitrogen) via reverse transfection following the manufacturer's instructions. The amount of DNA used for lipofection was 1 μg per transfection. In experiments with split base editors, 500 ng of each split were used. For simultaneous targeting experiments in HEK293Ts, 500 ng of plasmid encoding full-length BEs were transfected with 500 ng of plasmid with the sgRNA expression cassette when one sgRNA was expressed. Whenever two separate sgRNAs were transfected, 333.33 ng of plasmid encoding BEs was used with 333.33 ng of each sgRNA cassette. Transfection efficiency was routinely higher than 90% for HEK293T cells as determined by fluorescent microscopy following delivery of 1 μg of a GFP expression plasmid.

AAV vector production

AAV was produced according to the protocol described previously[84]. HEK293T cells were seeded onto 15-cm plates to be 80% confluent after

16 h and maintained in DMEM supplemented with 10% (v/v) FBS and 1% (v/v) penicillin/streptomycin. After 16 h, cells were transfected with 65 μg total of AAV vector plasmid (pAAV-CAG-N-ABE8e-SpRY-APPex17sgRNA, or pAAV- CAG-C-ABE8e-SpRY-APPex17sgRNA, or pAAV-CAG-GFP-KASH), pAAVrh10, and pHelper in a 1:1:1 mol ratio using PEI-max (pH = 8). XmaI digestion was used to confirm the integrity of the pAAV plasmids before transfection. Cell media was replaced 4 h after transfection. Cells were harvested 72 h after transfection by manual dissociation using a cell scraper and centrifuged at 1500 × *g* for 5 min at room temperature. The supernatant was collected into a fresh tube and mixed with 40% polyethylene glycol 8000 (Thermo Fisher) solution in a ratio of 4:1 by volume and stored overnight at 4 °C. Cell pellets were then resuspended in 2 mL of lysis buffer (50 mM Tris-HCl and 150 mM NaCl, pH 8.0) per plate. The next day, the supernatant solution was centrifuged at 1500 × *g* for 30 min at 4 °C. The pellets of the supernatant were resuspended in the same lysis buffer as described above and mixed with their respective cell lysates. These cell suspensions were then frozen in liquid nitrogen and thawed at 37 °C, for three freeze-thaw cycles to extract AAV vectors. Supernatants were then treated with 0.5% Triton X-100 (Thermo Fisher) and 50 units/mL Benzonase (Merck) shaking at 37 °C for 1 h. We then centrifuged the lysate at 10,000 × *g* for 15 min at room temperature. The resulting supernatant was overlaid onto an iodixanol density gradient using 15%, 25%, 40% and 60% Opti-Prep solution (Sigma-Aldrich) and the virus was isolated by ultracentrifugation at 266,910 × *g* at 18 °C. This step was repeated to perform a second gradient purification using iodixanol fractions of 30%, 40% and 60%. Following extraction, AAV was filter-dialyzed with 1X PBS containing 0.001% Tween-20 using an Amicon Ultra 100 kDa MWCO column (Merck). The titer of the purified AAV was determined, post-treatment with DNase I (Millipore Sigma), by quantitative real-time PCR using primers that amplify the bGH PolyA sequence (Table S3) and the SsoFast Evagreen mix (Bio-Rad). The virus was stored at −80 °C.

RT-PCR

RNA was harvested from cell pellets using the RNeasy Plus Mini Kit (Qiagen) according to manufacturer's instructions. cDNA synthesis was performed using the qScript cDNA Synthesis Kit (Quanta Biosciences) from 1 μg of RNA with cycling conditions performed as directed by the supplier. PCR was performed using KAPA2G Robust PCR kits from Kapa Biosystems. The 25 μL reactions used 25 ng of cDNA, Buffer A (5 μL), Enhancer (5 μL), dNTPs (0.5 μL), 10 μM forward primer (1.25 μL), 10 μM reverse primer (1.25 μL), KAPA2G Robust DNA Polymerase (0.5 U) and water (up to 25 μL). Cycling parameters were used a recommended by the manufacturer. The PCR products were visualized in 1% or 2% agarose gels stained with ethidium bromide and images were captured using a ChemiDoc-It2 (UVP). The DNA sequences of the primers for each target are provided in Table S3.

Densitometry analysis

Skipping efficiencies for screening of simultaneous sgRNA candidates were determined by densitometry analysis of the PCR products obtained from RT-PCR and analyzed by agarose gel electrophoresis using ImageJ software. After subtracting background noise, band intensity was compared using the following formula: % exon skipping = (Skipped Band Intensity)/(Non Skipped Band Intensity + Skipped Band Intensity) where band intensity is the sum of each pixel grayscale value within the selected area of the band.

Analysis of DNA editing rates

Genomic DNA was isolated using a DNeasy Blood and Tissue Kit (Qiagen) and PCR amplification was performed with KAPA2G Robust PCR kits (KAPA Biosystems) as described above, using 20–100 ng of template DNA and primers listed in Table S3.

Sanger sequencing of the PCR amplicons was performed by the Roy J. Carver Biotechnology Center at the University of Illinois at Urbana-Champaign. Base editing efficiencies were estimated by analyzing sequencing traces using EditR with the primers listed in Table S3.

Next-generation sequencing for RNA exon skipping and DNA amplicons

After cDNA synthesis (qScript, QuantaBio), amplicons were generated using KAPA HiFi HotStart (Roche), according to manufacturer's instructions with primers containing overhangs compatible with Nextera XT indexing (IDT). Primer sequences for all amplicons are listed in Table S3. Following validation of the quality of PCR products by gel electrophoresis, the PCR products were isolated using an AMPure XP PCR purification beads (Beckman Coulter). Indexed amplicons were then generated with a Nextera XT DNA Library Prep Kit (Illumina) and pooled. Libraries were sequenced with a MiSeq Nano Flow Cell for 251 cycles from each end of the fragment using a MiSeq Reagent Kit v2 (500-cycles). FASTQ files were created and demultiplexed using bcl2fastq v2.17.1.14 conversion software (Illumina). Deep sequencing was performed by the Roy J. Carver Biotechnology Center at the University of Illinois, Urbana, IL.

Exon skipping rates were quantified using the STAR RNA-Seq aligner on Galaxy. Forward and reverse reads were combined and aligned to the human reference genome (GRCh38, GenBank Assembly GCA_000001405.29) using STAR. 2-pass mapping was used for splice junction analysis with a MAPQ value of 60 for.bam files. Splice junctions formed were determined from STAR SJ.out.tab files where the percentage of a junction event was defined as the number of reads for the target junction divided by the total number of events at the specified junction. Sashimi plots for splice junctions were generated from the Integrative Genomics Viewer (IGV's) sashimi plot tool using the.-bam and.bai files outputted from RNA-STAR. These sashimi plots were illustrated in this manuscript by tracing the images generated from IGV in Adobe Illustrator.

For DNA amplicons, samples were isolated with the DNeasy Blood and Tissue Kit and the RNeasy Plus Mini Kit per manufacturer's specifications. Amplicons were generated by PCR with KAPA HiFi Hotstart using primers containing overhangs compatible with Nextera XT indexing primers listed in Table S3. Amplification, indexing, pooling, and sequencing was performed as described above. Base editing rates were quantified using CRISPResso2. Reads with average phred scores below 30 were removed and remaining reads were aligned to the expected amplicon sequences.

RNA-Seq

Following RNA isolation and analysis on a 1% agarose gel to determine purity, RNA seq libraries were prepped with the TrueSeq® mRNA library prep kit (Illumina) and samples were sequenced with a NovaSeq 6000 system (Illumina). For analysis, a quality check performed using FASTQC showed that average per-base read quality scores in all samples were above 34 and no adapter sequences were found, indicating high quality reads, requiring no trimming. The reads were then mapped to the human genome (hg38) using HISAT2, with over 96% of reads being mapped uniquely. These mapped reads were counted across human genes with featureCounts, using annotations of hg38 obtained from GENCODE. About 60% of reads were assigned to genes. Differential expression analysis was performed using Limma-voom[85] which first calculates TMM normalized counts-per-million (CPM) to account for compositional bias. In addition, genes expressed at very low levels (CPM lower than 0.5) were filtered out before performing differential expression analysis. For DEG, a DEG was defined as a gene with a Benjamini-Hochberg adjusted $p > 0.05$.

Off-target analysis

Off-target locations in the human genome (hg38) for the APP SA and SD 1 sgRNAs in Fig. S8A, B were identified using Cas-OFFinder[52]. Searches were limited to off-target sites with less than two mismatches with DNA/RNA bulge sizes less than zero. For both sgRNAs, all sites with one mismatch (two for SA sgRNA and one for SD 1 sgRNA) were selected, and the remaining sites had two mismatches. Locations were chosen in both coding and non-coding regions that had either NGG/NAG or NNN PAMs. Five genomic loci were selected for further analysis from the output of each search. The protospacer of each selected off-target site, its PAM and genomic coordinates are listed in Table S3 along with the corresponding primers used for DNA amplification. Targets were amplified and sequenced via NGS, as described above. Base editing rates were quantified using CRISPResso v2 as described above.

RT-qPCR

For qPCR, 50 ng of cDNA was used per sample. qPCR was performed with SsoFast™ EvaGreen® Supermix (Biorad) following manufacturer recommendations for both reaction setup and cycling conditions. 500 nM of qPCR primers were used per sample, and GAPDH was used as the housekeeping gene. Thermocycling and cycle threshold (ct) measurements was conducted on the CFX96™ qPCR instrument (Biorad). Gene expression levels were analyzed from ct values of the target genes and relative expression was quantified using the double-delta ct method[86]. All primers used for qPCR are listed under Table S3.

Western blot

Cells were lysed by resuspending pellets in 1X NuPAGE LDS Sample Buffer (Invitrogen) containing 2.5% β-mercaptoethanol. Samples were then boiled at 95 °C for 5 min, sonicated to shred genomic DNA, and boiled again at 95 °C for 5 min. Protein lysates were then electrophoresed using NuPAGE 4-12% Bis-Tris Gels and NuPAGE SDS Running Buffer (Invitrogen) for 2 h at 130 V and transferred to nitrocellulose membranes in Towbin transfer buffer (20 mM Tris-HCl pH 8.3, 192 mM glycine, and 10% (v/v) methanol, 1% SDS) for 2.5 h at 75 V in an ice chamber with constant agitation. Membranes were then blocked with 5% (v/v) non-fat dry milk in 1X Tris-buffered saline (TBS) (20 mM Tris-HCl, 150 mM NaCl, and 0.1%, pH 7.5) with 1% Tween 20 (TBS-T) for 2 h and then incubated overnight at 4 °C with primary antibodies: for Cas9 expression, mouse anti-Cas9, clone 7A9 (1:1000, Epigentek #A-9000) and rabbit anti-GAPDH (1:1000, Cell Signaling Technology #2118). After overnight incubation, the membranes were washed three times with 1x TBS-T and incubated with either 800CW goat anti-mouse fluorescent secondary (LI-COR # 926-32210), or 680RD donkey anti-rabbit fluorescent secondary (LI-COR #926-68073) in blocking solution for 1 h at room temperature at a 1:10,000 dilution. Membranes were washed three times with 1x TBS-T. All samples were then visualized using an Odyssey Imager (LI-COR). Band intensity was quantitated using ImageJ and normalized to GAPDH.

ELISA

To generate cells with editing at *APP* exon 17, BE(2)-M17 cells were transiently transfected via reverse transfection with lipofectamine 2000 containing 1 μg of pEFS-SpRY-ABE8e-T2A-Puro, a plasmid which also contained a U6 driven sgRNA expression cassette. For samples expressing multiple sgRNAs, 500 ng of each plasmid was used. 24 h after transfection, cell media was exchanged with media supplemented with 1 μg/mL puromycin and incubated for 36 h. Afterwards, cells were washed 3X with media without puromycin and incubated with this media for all further experiments unless otherwise noted.

For ELISA, cells were plated onto 10 cm dishes and grown to 100% confluency. After cells reached confluency, cell media was replaced and incubated for an additional 24 h. Media was then replaced with 10 mL OPTI-MEM supplemented with 1% penicillin/streptomycin and cells were incubated for 48 h. Cell supernatant was collected into 1.5 mL tubes, supplemented with 1X Halt™ Protease Inhibitor Cocktail (Thermo™ Scientific 78430) and centrifuged at 86 × *g* for 1 minute. The supernatant was collected, and an Aβ42 ELISA was performed on undiluted samples using the Ultrasensitive Aβ42 Human ELISA Kit (Thermo™ Scientific KHB3544) according to the manufacturer's instructions. Standards were diluted in OPTI-MEM supplemented with 1% penicillin/streptomycin and 1X Halt™ cocktail.

For total protein analysis, adhered cells were lysed with 1X RIPA buffer on ice with 1X Halt™ cocktail and incubated on ice for ten minutes. Cells were spun at 9362 × *g* for 10 min, and total protein content in the supernatant was quantified with the Pierce™ Bradford Protein Assay Kit (Thermo™ Scientific 23200) following manufacturer instructions.

After protein concentrations were quantified via ELISA, the concentration of Aβ42 was normalized to the total protein content of each sample by dividing each Aβ42 concentration by the total protein concentration. The value generated by each sample was normalized to its respective ROSA positive control.

Stereotaxic injections

All animal procedures were approved by the Illinois Institutional Animal Care and Use Committee at the University of Illinois and conducted in accordance with the National Institutes of Health (NIH) Guide for the Care and Use of Laboratory Animals.

Four to six week old transgenic B6.129-Tg(APPsw)40Btla/Mmjax mice (Jackson Laboratory #0034831-JAX) were injected with 5×10^9 vector genomes of each of AAVrh10-pAAV-CAG-N-ABE8e, pAAVrh10-CAG-C-ABE8e, and 5×10^8 vector genomes of AAVrh10-pAAV-CAG-KASH in 2 μl of PBS with 0.001% Tween-20 into each half of the hippocampus at coordinates −1.8 AP, ±1.5 ML, and 0.45 DV. Sex was not considered a variable in these studies.

Tissue harvesting and RNA purification

Mice were anesthetized using 3% isoflurane delivered through vaporizer in a closed chamber and transcardially perfused using 1 X PBS. The hippocampus was dissected, divided in 2 halves and each half was stored via flash freezing or in RNAlater (Invitrogen, AM7026).

For FACS, nuclei isolation was performed as previously described[87]. Briefly, tissues were homogenized in NF1 buffer using the KIMBLE Dounce Tissue Grinder (Sigma-Aldrich) per the manufacturer's instructions, strained through a 70 μm strainer into a 50 mL conical tube underlaid with a 1.2 M sucrose cushion, and centrifuged at 3900 G for 30 min at 4 °C. The supernatant was discarded and the pelleted nuclei were resuspended in 10 mL of NF1 buffer. Samples were spun 2X at 1600 G for 5 min at 4 °C and resuspended in 2 mL of FANS buffer. Cells were strained through a 35 μm strainer and incubated at 37 °C for 30 min with 0.5 μL Vybrant™ Dyecycle™ Ruby strain (Invitrogen, V10309) per mL of FANS buffer.

Harvested nuclei were sorted using a ThermoFisher Bigfoot Spectral Cell Sorter Cell Sorter (Roy J. Carver Biotechnology Center, University of Illinois, Urbana, IL). Cells were collected in FANS buffer. At least 10,000 cells or nuclei were sorted for each sample. Collected nuclei were diluted in FANS buffer with 1% wt/vol (g/mL) BSA and spun at 1600 G for 15 min at 4 °C. Supernatant was aspirated, and pelleted nuclei were isolated via the DNeasy Blood and Tissue Kit.

To perform downstream analysis on whole hippocampus samples, DNA and RNA samples were isolated with the DNeasy Blood and Tissue Kit and the RNeasy Plus Mini Kit per manufacturer's specifications, respectively. Prior to purification, brain tissue samples were homogenized in 1X PBS using a KIMBLE Dounce Tissue Grinder, diluted in the first buffer of each respective kit, and further isolated following the standard kit protocols.

For NGS on all DNA samples, Amplicons were generated by PCR with KAPA HiFi Hotstart using primers containing overhangs compatible with Nextera XT indexing primers listed in Table S3.

Amplification, indexing, pooling, and analysis of base editing rates was performed as described in the "*Next-Generation Sequencing for RNA Exon Skipping and DNA Amplicons*" section. For RNA analysis of exon skipping, cDNA synthesis and amplification for NGS was performed as described above, however, libraries or cDNA were sequenced with the MiSeq Bulk flow cell for 275 cycles from each end of the fragment using a MiSeq Reagent Kit v3 (500-cycles). Exon skipping was quantified with RNA-STAR as described above.

Statistics and reproducibility

GraphPad Prism version 9.1 (GraphPad Software, Inc.) software was used for statistical analysis. All experiments consisted of independent replicates. Test groups were compared using either student's t-test or a one-way ANOVA with Tukey's post hoc analysis. Statistical methods used for RNAseq are described within the section titled "*RNA-Seq*". No statistical method was used to predetermine the sample size. No data were excluded from the analysis. Experiments were performed with either biological duplicates or triplicates for each sample. The investigators were not blinded to allocation during experiments and outcome assessment.

Reporting summary

Further information on research design is available in the Nature Portfolio Reporting Summary linked to this article.

Data availability

All data needed to evaluate the conclusions is presented within the manuscript or in supplemental. The source data generated in this study are provided in the Supplementary Information/Source Data file. The high throughput sequencing data generated in this study has been deposited in the Gene Expression Omnibus database under accession code GSE246588. Source data are provided with this paper.

References

1. Anzalone, A. V., Koblan, L. W. & Liu, D. R. Genome editing with CRISPR–Cas nucleases, base editors, transposases and prime editors. *Nat. Biotechnol.* **38**, 824–844 (2020).
2. Adikusuma, F. et al. Large deletions induced by Cas9 cleavage. *Nature* **560**, E8–E9 (2018).
3. Leibowitz, M. L. et al. Chromothripsis as an on-target consequence of CRISPR–Cas9 genome editing. *Nat. Genet.* **53**, 895–905 (2021).
4. Haapaniemi, E., Botla, S., Persson, J., Schmierer, B. & Taipale, J. CRISPR–Cas9 genome editing induces a p53-mediated DNA damage response. *Nat. Med.* **24**, 927–930 (2018).
5. Tuladhar, R. et al. CRISPR-Cas9-based mutagenesis frequently provokes on-target mRNA misregulation. *Nat. Commun.* **10**, 4056 (2019).
6. Cox, D. B. T., Platt, R. J. & Zhang, F. Therapeutic genome editing: prospects and challenges. *Nat. Med.* **21**, 121–131 (2015).
7. Doudna, J. A. The promise and challenge of therapeutic genome editing. *Nature* **578**, 229–236 (2020).
8. Komor, A. C., Kim, Y. B., Packer, M. S., Zuris, J. A. & Liu, D. R. Programmable editing of a target base in genomic DNA without double-stranded DNA cleavage. *Nature* **533**, 420–424 (2016).
9. Gaudelli, N. M. et al. Programmable base editing of A• T to G• C in genomic DNA without DNA cleavage. *Nature* **551**, 464–471 (2017).
10. Gapinske, M. et al. CRISPR-SKIP: programmable gene splicing with single base editors. *Genome Biol.* **19**, 1–11 (2018).
11. Gapinske, M. et al. Targeting Duchenne muscular dystrophy by skipping DMD Exon 45 with base editors. *Mol. Ther. Nucleic Acids* **33**, 572–586 (2023).
12. Chai, A. C. et al. Single-swap editing for the correction of common Duchenne muscular dystrophy mutations. *Mol. Ther. Nucleic Acids* **32**, 522–535 (2023).
13. Yuan, J. et al. Genetic modulation of RNA splicing with a CRISPR-guided cytidine deaminase. *Mol. cell* **72**, 380–394.e7 (2018).
14. Webber, B. R. et al. Highly efficient multiplex human T cell engineering without double-strand breaks using Cas9 base editors. *Nat. Commun.* **10**, 5222 (2019).
15. Kluesner, M. G. et al. CRISPR-Cas9 cytidine and adenosine base editing of splice-sites mediates highly-efficient disruption of proteins in primary and immortalized cells. *Nat. Commun.* **12**, 2437 (2021).
16. Jinek, M. et al. A programmable dual-RNA–guided DNA endonuclease in adaptive bacterial immunity. *Science* **337**, 816–821 (2012).
17. Yang, B., Yang, L. & Chen, J. Development and application of base editors. *CRISPR J.* **2**, 91–104 (2019).
18. Winter, J. et al. Targeted exon skipping with AAV-mediated split adenine base editors. *Cell Discov.* **5**, 1–12 (2019).
19. Sibley, C. R., Blazquez, L. & Ule, J. Lessons from non-canonical splicing. *Nat. Rev. Genet.* **17**, 407–421 (2016).
20. Liu, Y. et al. Adenine base editor-mediated splicing remodeling activates non-canonical splice sites. *J. Biol. Chem.* **299**, 105442 (2023).
21. Jung, H. et al. Intron retention is a widespread mechanism of tumor-suppressor inactivation. *Nat. Genet.* **47**, 1242–1248 (2015).
22. Dvinge, H. & Bradley, R. K. Widespread intron retention diversifies most cancer transcriptomes. *Genome Med.* **7**, 1–13 (2015).
23. Hsu, T. Y.-T. et al. The spliceosome is a therapeutic vulnerability in MYC-driven cancer. *Nature* **525**, 384–388 (2015).
24. Julia, T. & Goate, A. M. Genetics of β-amyloid precursor protein in Alzheimer's disease. *Cold Spring Harbor Perspect. Med.* **7**, a024539 (2017).
25. Chang, J. L. et al. Targeting amyloid-β precursor protein, APP, splicing with antisense oligonucleotides reduces toxic amyloid-β production. *Mol. Ther.* **26**, 1539–1551 (2018).
26. Scheltens, P. et al. Alzheimer's disease. *Lancet* **388**, 505–517 (2016).
27. Gouras, G. K., Olsson, T. T. & Hansson, O. β-Amyloid peptides and amyloid plaques in Alzheimer's disease. *Neurotherapeutics* **12**, 3–11 (2015).
28. Karran, E. & De Strooper, B. The amyloid hypothesis in Alzheimer disease: new insights from new therapeutics. *Nat. Rev. Drug Discov.* **21**, 306–318 (2022).
29. Duan, Y. et al. Brain-wide Cas9-mediated cleavage of a gene causing familial Alzheimer's disease alleviates amyloid-related pathologies in mice. *Nat. Biomed. Eng.* **6**, 168–180 (2022).
30. Hampel, H. et al. The amyloid-β pathway in Alzheimer's disease. *Mol. psychiatry* **26**, 5481–5503 (2021).
31. Kleinstiver, B. P. et al. Engineered CRISPR-Cas9 nucleases with altered PAM specificities. *Nature* **523**, 481–485 (2015).
32. Hua, K., Tao, X., Yuan, F., Wang, D. & Zhu, J.-K. Precise A· T to G· C base editing in the rice genome. *Mol. Plant* **11**, 627–630 (2018).
33. Zhang, C. et al. Expanding the base editing scope to GA and relaxed NG PAM sites by improved xCas9 system. *Plant Biotechnol. J.* **18**, 884 (2020).
34. Hu, J. H. et al. Evolved Cas9 variants with broad PAM compatibility and high DNA specificity. *Nature* **556**, 57–63 (2018).
35. Goldberg, G. W. et al. Engineered dual selection for directed evolution of SpCas9 PAM specificity. *Nat. Commun.* **12**, 349 (2021).
36. Li, J. et al. Genome editing mediated by SpCas9 variants with broad non-canonical PAM compatibility in plants. *Mol. Plant* **14**, 352–360 (2021).
37. Walton, R. T., Christie, K. A., Whittaker, M. N. & Kleinstiver, B. P. Unconstrained genome targeting with near-PAMless engineered CRISPR-Cas9 variants. *Science* **368**, 290–296 (2020).
38. Scotti, M. M. & Swanson, M. S. RNA mis-splicing in disease. *Nat. Rev. Genet.* **17**, 19–32 (2016).

39. Koblan, L. W. et al. Improving cytidine and adenine base editors by expression optimization and ancestral reconstruction. *Nat. Biotechnol.* **36**, 843–846 (2018).
40. Thuronyi, B. W. et al. Continuous evolution of base editors with expanded target compatibility and improved activity. *Nat. Biotechnol.* **37**, 1070–1079 (2019).
41. Yu, Y. et al. Cytosine base editors with minimized unguided DNA and RNA off-target events and high on-target activity. *Nat. Commun.* **11**, 2052 (2020).
42. Neugebauer, M. E. et al. Evolution of an adenine base editor into a small, efficient cytosine base editor with low off-target activity. *Nat. Biotechnol.* **41**, 673–685 (2023).
43. Gaudelli, N. M. et al. Directed evolution of adenine base editors with increased activity and therapeutic application. *Nat. Biotechnol.* **38**, 892–900 (2020).
44. Richter, M. F. et al. Phage-assisted evolution of an adenine base editor with improved Cas domain compatibility and activity. *Nat. Biotechnol.* **38**, 883–891 (2020).
45. Chen, L. et al. Engineering a precise adenine base editor with minimal bystander editing. *Nat. Chem. Biol.* **19**, 101–110 (2023).
46. Garcia-Blanco, M. A., Baraniak, A. P. & Lasda, E. L. Alternative splicing in disease and therapy. *Nat. Biotechnol.* **22**, 535–546 (2004).
47. Liu, Y. et al. Genome-wide screening for functional long noncoding RNAs in human cells by Cas9 targeting of splice sites. *Nat. Biotechnol.* **36**, 1203–1210 (2018).
48. Grymová, T., Grodecká, L., Souček, P. & Freiberger, T. SERPING1 exon 3 splicing variants using alternative acceptor splice sites. *Mol. Immunol.* **107**, 91–96 (2019).
49. Jung, H., Lee, K. S. & Choi, J. K. Comprehensive characterisation of intronic mis-splicing mutations in human cancers. *Oncogene* **40**, 1347–1361 (2021).
50. Li, R. et al. Amyloid β peptide load is correlated with increased β-secretase activity in sporadic Alzheimer's disease patients. *Proc. Natl Acad. Sci. USA* **101**, 3632–3637 (2004).
51. Zhang, Y.-W., Thompson, R., Zhang, H. & Xu, H. APP processing in Alzheimer's disease. *Mol. Brain* **4**, 1–13 (2011).
52. Bae, S., Park, J. & Kim, J.-S. Cas-OFFinder: a fast and versatile algorithm that searches for potential off-target sites of Cas9 RNA-guided endonucleases. *Bioinformatics* **30**, 1473–1475 (2014).
53. Thal, D. R., Capetillo-Zarate, E., Del Tredici, K. & Braak, H. The development of amyloid β protein deposits in the aged brain. *Sci. Aging Knowl. Environ.* **2006**, re1–re1 (2006).
54. Macias, M. P. et al. A cellular model of amyloid precursor protein processing and amyloid-β peptide production. *J. Neurosci. Methods* **223**, 114–122 (2014).
55. Lamb, B. T. et al. Altered Metabolism of Familial Alzheimer's Disease-Linked Amyloid Precursor Protein Variants in Yeast Artificial Chromosome Transgenic Mice. *Hum. Mol. Genet.* **6**, 1535–1541 (1997).
56. Cearley, C. N. & Wolfe, J. H. Transduction characteristics of adeno-associated virus vectors expressing cap serotypes 7, 8, 9, and Rh10 in the mouse brain. *Mol. Ther.* **13**, 528–537 (2006).
57. Lim, C. K. et al. Treatment of a mouse model of ALS by in vivo base editing. *Mol. Ther.* **28**, 1177–1189 (2020).
58. Levy, J. M. et al. Cytosine and adenine base editing of the brain, liver, retina, heart and skeletal muscle of mice via adeno-associated viruses. *Nat. Biomed. Eng.* **4**, 97–110 (2020).
59. Li, J. et al. Therapeutic exon skipping through a CRISPR-guided cytidine deaminase rescues dystrophic cardiomyopathy in vivo. *Circulation* **144**, 1760–1776 (2021).
60. Kim, Y. J. et al. Exon-skipping antisense oligonucleotides for cystic fibrosis therapy. *Proc. Natl Acad. Sci. USA* **119**, e2114858118 (2022).
61. Sud, R., Geller, E. T. & Schellenberg, G. D. Antisense-mediated exon skipping decreases tau protein expression: a potential therapy for tauopathies. *Mol. Ther. Nucleic Acids* **3**, e204 (2014).
62. Yamamura, T. et al. Development of an exon skipping therapy for X-linked Alport syndrome with truncating variants in COL4A5. *Nat. Commun.* **11**, 2777 (2020).
63. Zhu, X.-x. et al. Adenine base-editing-mediated exon skipping induces gene knockout in cultured pig cells. *Biotechnol. Lett.* **44**, 59–76 (2022).
64. Liu, J.-q. & Li, T. CRISPR-Cas9-mediated loss-of-function screens. *Front. Life Sci.* **12**, 1–13 (2019).
65. Aartsma-Rus, A. The future of exon skipping for Duchenne muscular dystrophy. *Hum. Gene Ther.* **34**, 372–378 (2023).
66. Kole, R. & Krieg, A. M. Exon skipping therapy for Duchenne muscular dystrophy. *Adv. Drug Deliv. Rev.* **87**, 104–107 (2015).
67. Xue, K. & MacLaren, R. E. Antisense oligonucleotide therapeutics in clinical trials for the treatment of inherited retinal diseases. *Expert Opin. Investig. Drugs* **29**, 1163–1170 (2020).
68. Dulla, K. et al. Antisense oligonucleotide-based treatment of retinitis pigmentosa caused by USH2A exon 13 mutations. *Mol. Ther.* **29**, 2441–2455 (2021).
69. Gee, P. et al. Extracellular nanovesicles for packaging of CRISPR-Cas9 protein and sgRNA to induce therapeutic exon skipping. *Nat. Commun.* **11**, 1334 (2020).
70. Kenjo, E. et al. Low immunogenicity of LNP allows repeated administrations of CRISPR-Cas9 mRNA into skeletal muscle in mice. *Nat. Commun.* **12**, 7101 (2021).
71. Chemello, F. et al. Precise correction of Duchenne muscular dystrophy exon deletion mutations by base and prime editing. *Sci. Adv.* **7**, eabg4910 (2021).
72. Happi Mbakam, C. et al. Prime editing strategies to mediate exon skipping in DMD gene. *Front. Med.* **10**, 1128557 (2023).
73. Tao, J., Bauer, D. E. & Chiarle, R. Assessing and advancing the safety of CRISPR-Cas tools: from DNA to RNA editing. *Nat. Commun.* **14**, 212 (2023).
74. Sharpe, J. J. & Cooper, T. A. Unexpected consequences: exon skipping caused by CRISPR-generated mutations. *Genome Biol.* **18**, 1–4 (2017).
75. Jeong, Y. K., Song, B. & Bae, S. Current status and challenges of DNA base editing tools. *Mol. Ther.* **28**, 1938–1952 (2020).
76. Slesarenko, Y. S., Lavrov, A. V. & Smirnikhina, S. A. Off-target effects of base editors: what we know and how we can reduce it. *Curr. Genet.* **68**, 39–48 (2022).
77. Park, S. & Beal, P. A. Off-target editing by CRISPR-guided DNA base editors. *Biochemistry* **58**, 3727–3734 (2019).
78. Liang, P. et al. Genome-wide profiling of adenine base editor specificity by EndoV-seq. *Nat. Commun.* **10**, 67 (2019).
79. Jin, S. et al. Cytosine, but not adenine, base editors induce genome-wide off-target mutations in rice. *Science* **364**, 292–295 (2019).
80. Zuo, E. et al. Cytosine base editor generates substantial off-target single-nucleotide variants in mouse embryos. *Science* **364**, 289–292 (2019).
81. Blencowe, B. J. Exonic splicing enhancers: mechanism of action, diversity and role in human genetic diseases. *Trends Biochem. Sci.* **25**, 106–110 (2000).
82. Cartegni, L., Wang, J., Zhu, Z., Zhang, M. Q. & Krainer, A. R. ESE-finder: a web resource to identify exonic splicing enhancers. *Nucleic Acids Res.* **31**, 3568–3571 (2003).
83. Qiu, H. et al. Efficient exon skipping by base-editor-mediated abrogation of exonic splicing enhancers. *Cell Rep.* **42**, 113340, (2023).
84. Crosson, S. M., Dib, P., Smith, J. K. & Zolotukhin, S. Helper-free production of laboratory grade AAV and purification by iodixanol density gradient centrifugation. *Mol. Ther. Methods Clin. Dev.* **10**, 1–7 (2018).
85. Law, C. W., Chen, Y., Shi, W. & Smyth, G. K. voom: precision weights unlock linear model analysis tools for RNA-seq read counts. *Genome Biol.* **15**, 1–17 (2014).

86. Livak, K. J. & Schmittgen, T. D. Analysis of relative gene expression data using real-time quantitative PCR and the 2− ΔΔCT method. *Methods* **25**, 402–408 (2001).
87. Nott, A., Schlachetzki, J. C., Fixsen, B. R. & Glass, C. K. Nuclei isolation of multiple brain cell types for omics interrogation. *Nat. Protoc.* **16**, 1629–1646 (2021).

Acknowledgements

We thank the DNA Services staff of the Roy J. Carver Biotechnology Center at the University of Illinois, particularly Alvaro Hernandez and Chris Wright, for their support with DNA and RNA sequencing. We thank Siva Mayandi of the Roy J. Carver Biotechnology Center Cytometry and Microscopy to Omics facility at the University of Illinois for his support with FACS. This work was supported by the National Institutes of Health grants 1U01NS122102 (T.G. and P.P.P.), 1R01NS123556 (T.G. and P.P.P.), 1R01GM141296 (T.G. and P.P.P.), 1R01GM127497 (P.P.P.), 1R01GM131272 (P.P.P.), the Muscular Dystrophy Association grant MDA602798 (T.G. and P.P.P.), the American Heart Association grant 17SDG33650087 (P.P.P.), the Parkinson's Disease Foundation grant PF-IMP-1950 (T.G. and P.P.P.) and the Simons Foundation grant 887187 (T.G. and P.P.P). J.W. was supported by the Northwestern University Clinical and Translational Science Institute, grant UL1TR001422. A.M. was supported by the National Institute of Biomedical Imaging and Bioengineering of the National Institutes of Health under Award Number T32EB019944. The content is solely the responsibility of the authors and does not necessarily represent the official views of the National Institutes of Health.

Author contributions

A.M., S.S., T.G., and P.P. conceived of the study; A.M., S.S., J.W., G.E., M.G., D.S., W.S.W, N.G., M.G., M.S., A.Z., and H.M. designed and performed experiments; A.N. and S.M. assisted with bioinformatic analysis of RNAseq data. A.M., T.G., and P.P. wrote the manuscript with input from all authors.

Competing interests

P.P.P., M.G., and J.W. are named inventors in pending patent application US17/260,828 filed by the University of Illinois. Methods for exon skipping and AAV-mediated delivery of base editors are covered in the patent application. The remaining authors declare no competing interests.

Additional information

Supplementary information The online version contains supplementary material available at https://doi.org/10.1038/s41467-024-54529-y.

Correspondence and requests for materials should be addressed to Pablo Perez-Pinera.

Peer review information *Nature Communications* thanks the anonymous reviewers for their contribution to the peer review of this work. A peer review file is available.